RSC Advances

Accepted Manuscript

ROYAL SOCIETY OF CHEMISTRY

rsc.li/rsc-advances

Journal Name

ARTICLE

Nonlinear transmittance and optical power limiting in Magnesium ferrite nanoparticles: effects of laser pulsewidth and particle size†

Received 00th January 20xx,
Accepted 00th January 20xx

DOI: 10.1039/x0xx00000x

www.rsc.org/

Sreekanth Perumbilavil,‡[a,b] Kishore Sridharan,*[c] Ann Rose Abraham,[b] Harsha P Janardhanan,[b] Nandakumar Kalarikkal[b,d] and Reji Philip[a]

We report comparative measurements of size dependent nonlinear transmission and optical power limiting in nanocrystalline magnesium ferrite ($MgFe_2O_4$) particles excited by short (nanosecond) and ultrashort (femtosecond) laser pulses. Standard sol-gel technique is employed to synthesize particles in the size range of 10-50 nm, using polyvinyl alcohol as the chelating agent. Structure and morphology of the samples is studied using X-ray diffraction, scanning electron microscopy and transmission electron microscopy. Growth of the particles in time is tracked through Fourier transform infrared spectroscopy. Nonlinear transmission measurements have been carried out using the open aperture Z-scan technique employing 532 nm, 5 nanosecond pulses and 800 nm, 100 femtosecond pulses, respectively. The measured optical nonlinearity is primarily of a reverse saturable absorption (RSA) nature, arising mostly from excited state absorption for nanosecond excitation, and two-photon absorption for femtosecond excitation. The optical limiting efficiency is found to increase with particle size for both cases. The calculated nonlinear parameters indicate that these materials are potential candidates for optical limiting applications.

Introduction

Transition-metal oxides are considered to be a most fascinating class of materials among inorganic solids because of the wide variety of structures and properties they exhibit.[1] Spinel ferrites (chemical composition = MFe_2O_4) are a small group of transition-metal oxide compounds which are mainly derived from magnetite (Fe_3O_4). They are tunable magnetic systems having a face-centered cubic structure with a large unit cell in which M^{2+} and Fe^{3+} cations coordinate with the oxygen atoms at tetrahedral and octahedral sites, respectively.[2] When bulk spinel ferrites are scaled down to nanometer range, modifications happen in the surface/interface, electronic states and magnetic interactions, which lead to varied saturation magnetization, coercivity, spin-canting and hysteresis loop.[3-5] Due to the low cost and abundance of the precursors, nanosized spinel ferrites continue to evoke interest in researchers for understanding their intrinsic magnetic properties, which can be tuned for wide range of applications such as high-density data storage, ferrofluids, sensors, spintronics, magnetocaloric refrigeration, heterogeneous catalysis, magnetic labelling in immunoassays, guided drug delivery, magnetic resonance imaging and hyperthermia of cancer cells.[6-14]

Magnesium ferrite ($MgFe_2O_4$) is soft magnetic in nature and is an n-type semiconductor.[15] Due to the redistribution of iron ions between A- and B-sites, the theoretical value of magnetization in $MgFe_2O_4$ nanoparticles (referred hereafter as MgF NPs) is predicted to be two times higher than its bulk.[16] MgF NPs are capable of exhibiting superparamagnetism,[15, 17, 18] and have been utilized for applications in catalysis,[19, 20] sensors,[21-24] and magnetic hyperthermia.[25] Study on the magneto-dielectric properties of MgF NPs have indicated their potential for high frequency antennas, owing to their low magnetic and dielectric tangents.[26]

Magnetic nanoparticles suspended in a liquid medium (ferrofluids) under externally applied magnetic field exhibit unique magneto-optical properties, which can be utilized for applications such as optical shutters, switches and tunable polarizing or phase changing elements.[27] Similarly, ferrofluids and other magnetic nanoparticles have been exploited for applications in optical limiting.[28-30] Optical limiters are devices capable of protecting the human eye or a sensor from intense laser radiation and it would be very interesting to magnetically control the nonlinear optical properties.[31] In the recent past, we have reported the optical limiting properties of spinel ferrites such as $NiFe_2O_4$, $CoFe_2O_4$, $ZnFe_2O_4$ and mixed zinc

[a] Ultrafast and Nonlinear Optics Lab, Light and Matter Physics Group, Raman Research Institute, C.V. Raman Avenue, Sadashivanagar, Bangalore 560080, India
[b] School of Pure and Applied Physics, Mahatma Gandhi University, Kottayam 686560, India
[c] Department of Physics, National Institute of Technology Karnataka, P.O. Srinivasnagar, Surathkal, Mangaluru 575025, India
Email: kishore@nitk.edu.in, sridharankishore@gmail.com Tel: 0824 247 3275
[d] International and Interuniversity Centre for Nanoscience and Nanotechnology, Mahatma Gandhi University, Kottayam 686560, India
‡ Present address: Optics Laboratory, Tampere University of Technology, FI-33101 Tampere, Finland
Electronic Supplementary Information (ESI) available: [plots showing the variation in particle size, lattice size, unit cell volume and bandgap energy as a function of annealing temperature]. See DOI: 10.1039/x0xx00000x

ferrites.[32-34] However, optical nonlinearities of other spinel ferrites still remain unexplored, and in particular, there are no reports till date on the study of the optical nonlinearity of spinel ferrites in the ultrashort laser excitation regime, where femtosecond laser pulses are used for excitation. Therefore, in the present work we compare the nonlinear optical properties of MgF NPs excited using nanosecond (ns) and femtosecond (fs) laser pulses, and show that when the optical fluences are approximately of the same order, about three to four orders of magnitude increase in optical intensity is required for fs excitation, to match the nonlinear transmittance achieved by ns excitation.

Experimental

Sol-gel technique was employed in the synthesis of MgF NPs using polyvinyl alcohol (PVA) as the chelating agent. In a typical process, 0.1 M of magnesium nitrate ($Mg(NO_3)_2.6H_2O$, Fisher Scientific, 99.9% purity) solution was uniformly mixed with 0.2 M of iron (III) nitrate ($Fe(NO_3)_3.9H_2O$, Fisher Scientific, 99.99% purity) solution. PVA was added under vigorous stirring to the stoichiometrically mixed precursor solution with a weight equal to the weight of metal ions in the solution. After ensuring the dissolution of PVA, the solution was evaporated at 60 ^{o}C till it gradually turned into a viscous sol and then to a dark brown gel. The gel was calcined at different temperatures for 150 min in a furnace and the resulting product was finely ground using a mortar and pestle to obtain MgF NPs. The samples calcined at 300, 400, 500, 600 and 700 ^{o}C were named as MgF1, MgF2, MgF3, MgF4 and MgF5, respectively.

Powder X-ray diffraction (XRD) patterns of the samples were recorded using an X-ray diffractometer (PANalytical, *X'PertPRO*) with Cu Kα radiation in the range 2θ = 10 – 80^{o}. Field emission scanning electron microscopy (FESEM) were performed on a Sigma (*ZIESS*) microscope equipped with a field emission gun. The samples for FESEM analysis were prepared by drop casting an ultrasonically dispersed solution containing 5 mg MgF NPs (MgF1–MgF5) in 5 ml ethanol on a clean Fluorine doped tin oxide (FTO, 1×1 cm dimension) glass which was dried overnight in a dry oven at 60 ^{o}C. The dried FTO glasses were placed on a carbon self-adhesive tape struck over an aluminium holder and sputter coated with a thin layer of gold to minimize charging. High-resolution transmission electron microscopy images and selected area electron diffraction patterns were obtained using a JEOL (*JEM 2100*) microscope. The UV–Vis absorption spectra were recorded using a spectrophotometer (Shimadzu, *UV-1800*) at room temperature.

The open aperture Z-scan technique was employed to measure the nonlinear optical transmission of the as synthesized nanoparticles. Experiments were done using 5 ns pulses (at 532 nm) obtained from a frequency-doubled Nd:YAG laser (Continuum, *Minilite*) and 100 fs pulses (at 800 nm) obtained from a regeneratively amplified Ti: Sapphire laser (Spectra Physics, *TSA-10*). Samples were prepared by dispersing the synthesized nanoparticles in dimethyl formamide (DMF). The dispersions were taken in a 1 mm thick glass cuvette and mounted on a programmable linear translation stage. By appropriate dilution, the linear transmittance of all measured samples was adjusted to be 55% at both the wavelengths (532 and 800 nm). Laser beams were focused using a plano-convex lens of 10.75 cm focal length, and samples were translated along the beam axis (Z axis) through the focal point. At each position (Z) the sample experiences a different laser fluence, and the corresponding transmission is measured using a pyroelectric detector (Rjp 735, Laser Probe Inc.). The normalized transmission plotted against Z gives the Z-scan curve, from which the transmission of the sample as a function of input fluence (or intensity) can be deduced. The nonlinear optical parameters are calculated by numerical fitting of this data to the nonlinear transmission equations. The laser pulse repetition rate in all our measurements is very low, at approximately one pulse in 5 s. For 800 nm excitation this is achieved by using an electronically controlled fast mechanical shutter in the beam path, and for 532 nm external triggering of Q-switch is employed.

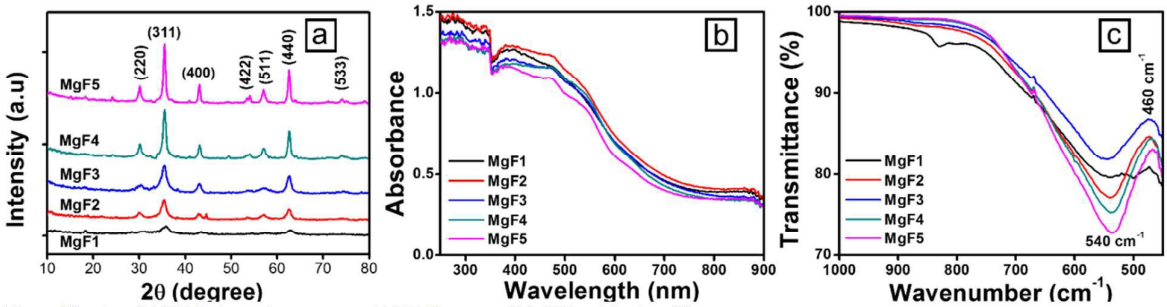

Fig. 1 (a) X-ray diffraction, (b) UV-Vis absorption spectra and (c) FT-IR spectra of MgF NPs calcined at different temperatures.

Results and discussion

The X-ray diffraction (XRD) patterns obtained on the MgF NPs calcined at different temperatures are shown in Fig. 1a. All the diffraction peaks can be indexed to cubic spinel structure of $MgFe_2O_4$ (JCPDS card no. 17-0464) with a space group *Fd-3m*.[35] The average particle size calculated from the dominant XRD peaks using the Debye-Scherer equation,[36] are 11 nm, 15 nm, 20 nm, 38 nm and 50 nm for MgF1, MgF2, MgF3, MgF4 and

MgF5, respectively. As reported in literature, the increase in the calcination temperature decreases the XRD peak broadening, due to which the particle size and crystallinity increases.[37, 38] Fig. S1a (ESI†) presents the particle size plotted as a function of annealing temperature. The smooth and steady increase in the particle size of MgF NPs indicates that the experimental condition and annealing temperature can be varied to obtain NPs of desired sizes. The lattice parameter and the unit cell volume of the MgF NPs samples were determined using unit cell parameter software. The calculated lattice parameters and unit cell volume as a function of annealing temperature are presented in Fig. S1b and S1c (ESI†). The insets of the figures show the unit cell volume plotted as a function of annealing temperature and particle size. UV-Vis absorption spectra of MgF NPs calcined at different temperatures are shown in Fig. 1b. The spectrum shows strong absorption in the UV and visible light region

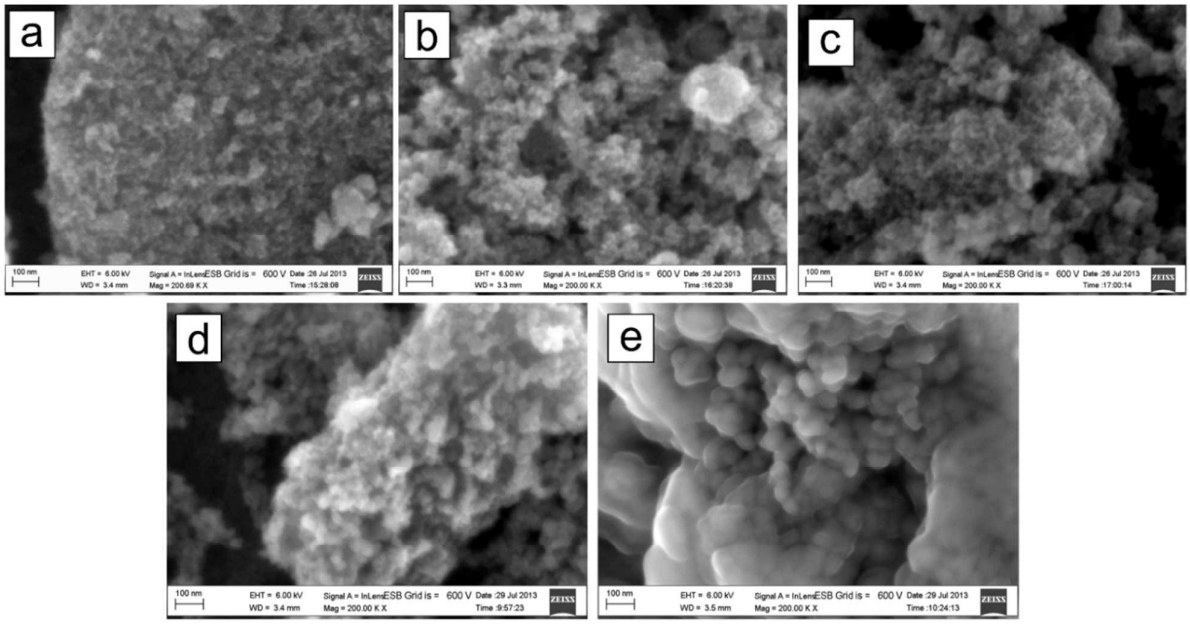

Fig. 2 SEM micrographs of (a) MgF1, (b) MgF2, (c) MgF3, (d) MgF4 and (e) MgF5 samples at a magnification of 200 KX.

which extends up to the IR region, but does not show any definite absorption peak.[39] The bandgap energy (E_g) was calculated from the expression for the absorption coefficient (α) near the bandedge, assuming a direct band gap using the Tauc relation.[40, 41] The E_g values obtained (4.08 eV, 3.9 eV, 3.82 eV, 3.73 eV and 3.64 eV for MgF1, MgF2, MgF3, MgF4 and MgF5, respectively) plotted against annealing temperature and particle size are presented in Fig. S1d (ESI†). The obtained values indicate that E_g decreases with increase in the particle size. Fourier Transformed Infrared spectra (FT-IR) of the calcined MgF NPs are shown in Fig. 1c. Literature reports indicate that the vibrations of ions in the spinel ferrite crystal lattice are mainly observed in the range of 400-1000 cm^{-1}.[42, 43]

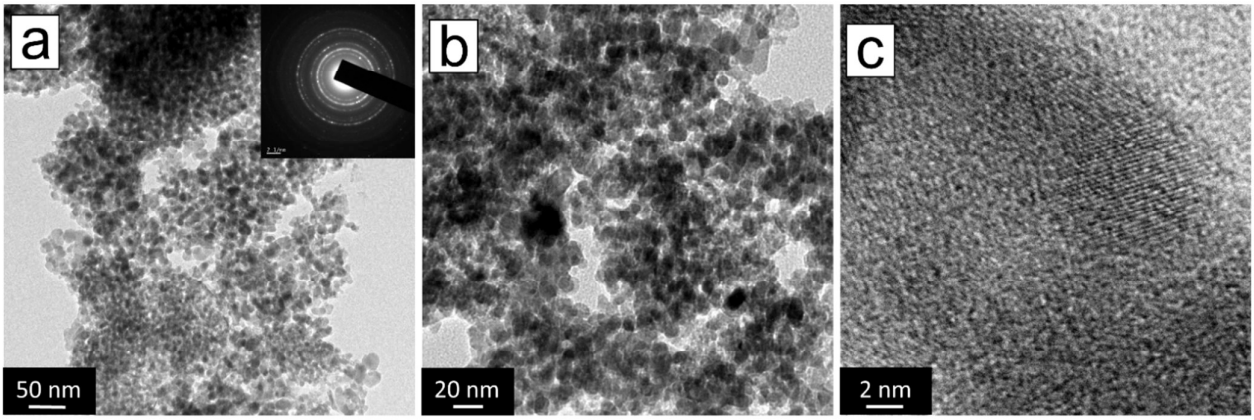

Fig. 3 TEM images of MgF NPs (MgF1, calcined at 300 °C) obtained under two different magnifications and (c) the HRTEM image obtained by scanning the area of a single MgF nanoparticle. SAED pattern corresponding to the TEM image shown in (a) is presented in the inset.

Journal Name

ARTICLE

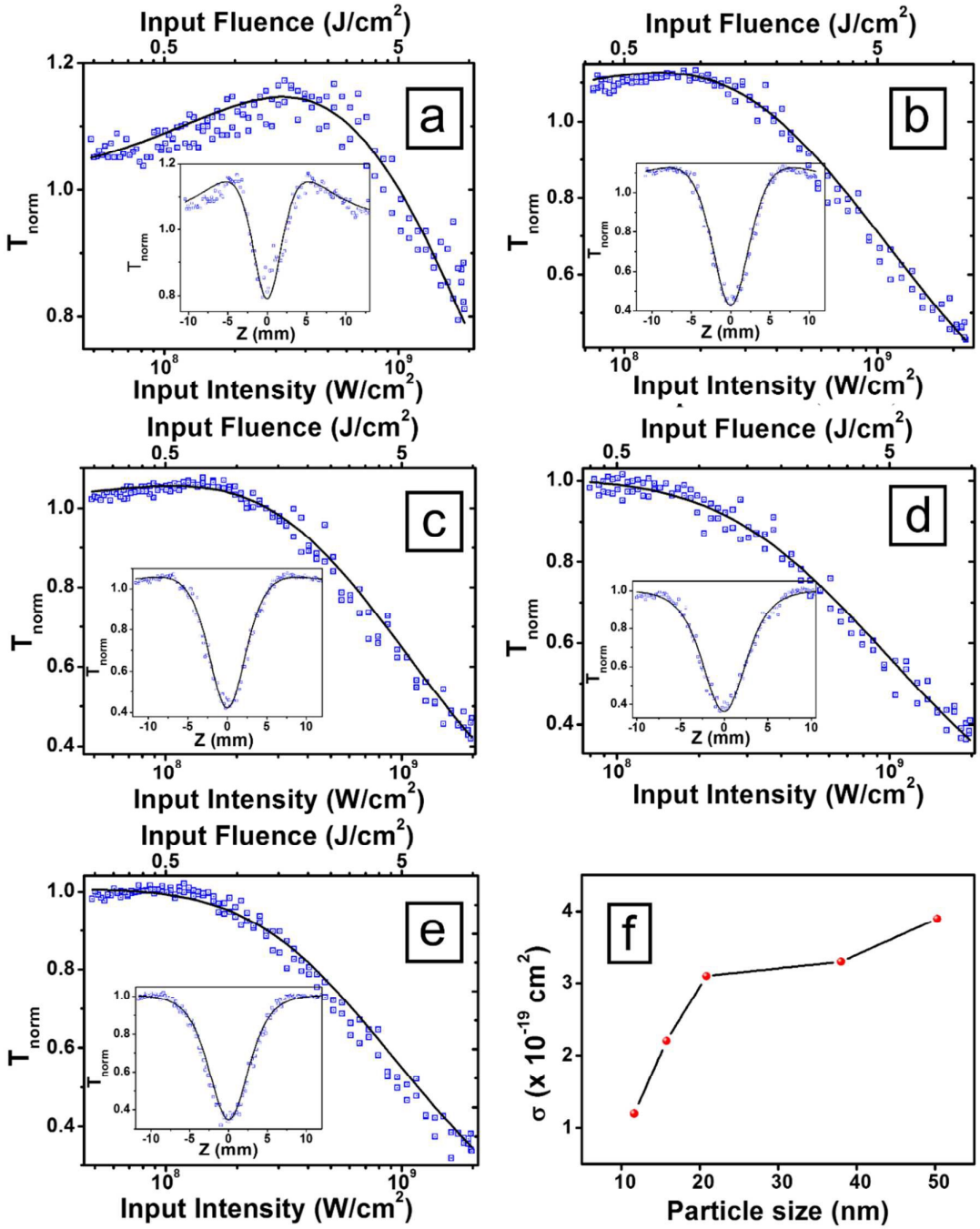

Fig. 4 Normalized transmission of the samples plotted as a function of input fluence and intensity, deduced from the open aperture Z-scans given in the insets. (a) MgF1, (b) MgF2, (c) MgF3, (d) MgF4 and (e) MgF5. Excitation is by 5 ns, 532 nm laser pulses, of energy 55 μJ. Open circles are data points and solid curves are numerical fits to the data using equation 1. (f) Correlation between particle size and excited state absorption cross section (σ). The line is a guide to the eye.

Journal Name

ARTICLE

Formation of spinel ferrites can be attributed to the intrinsic stretching vibrations due to (i) interaction of oxygen atom with the metal cations (Mg^{2+}) in the tetrahedral sites (observed in the range 540-560 cm^{-1}) and (ii) interaction of oxygen atom with metal cations (Fe^{3+}) at the octahedral sites (observed in the range 431-460 cm^{-1}). The FTIR spectra exhibits well-established strong absorption bands at ~540 and ~460 cm^{-1} for MgF5 sample calcined at 700 ^{o}C indicating the formation of magnesium ferrite. The 540 cm^{-1} band is attributed to the Fe–O stretching vibration (ν_1 mode) and the 460 cm^{-1} band corresponds to the O–Fe–O deformation vibration (ν_2 mode).[44, 45] The band in MgF1 appearing at ~860 cm^{-1} can be associated to the incomplete decomposition of PVA which fade out while MgF NPs are calcined at temperatures above 400 ^{o}C. On the other hand, the small kink appearing at ~670 cm^{-1} can be attributed to the characteristic vibration of the Mg–O bond.[46, 47] Annealing temperature variations were found to have a direct impact on the IR spectra of the MgF NPs in the form of vertical peak shifts (increase/decrease in Transmission %) due to the redistribution of the metal cations. However, the IR spectra of MgF NPs did not exhibit any monotonic dependence on annealing temperature, which can be attributed to tetrahedral defects and adsorbed species formed on the particle surfaces and variations in the particle size.[48]

Scanning Eelectron Microscopy (SEM) images of the calcined MgF NPs obtained at a constant magnification of 200 KX are shown in Fig. 2. Since the particle sizes calculated from XRD range between 10-50 nm, the working distance (WD) was reduced to 3.4 mm (since shorter WD allows for higher resolution) for clearly imaging the nanometer scale particles through FESEM at a constant magnification of 200 KX, as shown in Fig. 2. We observed electron beam induced sample damage at high acceleration voltages owing to which it was optimized and fixed at 6 kV. As observed from Fig. 2, there is a prominent increase in the particle size of MgF5 (calcined at 700 ^{o}C, Fig. 2e) in comparison to MgF1 (calcined at 300 ^{o}C, Fig. 2a). This indicates that the particle size indeed increases with respect to increase in calcination temperature, and these results are consistent with the XRD results and the particle size calculations obtained using the Debye-Scherrer's equation. TEM analysis performed on the as-prepared MgF NPs calcined at 300 ^{o}C (MgF1) are presented in Fig. 3. As seen from Fig. 3a and 3b, the particles are quite small with an average size ranging between 8-15 nm. The SAED pattern corresponding to the TEM image in Fig. 3a shows a spot type ring pattern, revealing the crystalline spinel structure of $MgFe_2O_4$. The lattice fringes seen from the HRTEM image in Fig. 3c indicates the crystalline structure of spinel MgF NPs. However, the fringes are not consistently clear which might be due to the incomplete removal of PVA (chelating agent).

Open aperture Z-scan curves measured for calcined MgF NPs using short (5 ns) and ultrashort (100 fs) laser pulses, and the corresponding fluence vs. normalized transmittance curves calculated from the Z-scan curves, are shown in Figs. 4 and 5, respectively. The input laser pulse energies used are 55 μJ for 5 ns excitation, and 7 μJ for 100 fs excitation. The Z-scan traces show decreased transmittance at higher laser fluences, indicating the occurrence of nonlinear absorption.

The nonlinear optical transmission of material media typically arise from saturable absorption (SA) and/or reverse saturable absorption (RSA). Occurrence of RSA is dependent on the material and excitation wavelength, and can happen due to phenomena such as excited state absorption (ESA), free carrier absorption, and two-photon absorption. It may be noted that sequential ESA and three-photon absorption can occur at high fluences and intensities. Therefore, by numerically fitting the measured data to standard nonlinear transmission equations, we have determined the prominent order of the nonlinearity. Best fits to the data were obtained for a combined process involving SA and ESA for ns excitation, and SA and two-photon absorption (2PA) for fs excitation, showing that the nonlinearity is primarily of the third order. Sequential ESA and three-photon absorption, if occurring, are relatively weak in comparison. The SA effect is prominently visible for MgF1 (see Fig. 4a) and it progressively decreases as the particle size increases (Fig. 4b to 4e). An important point to note here is that while the fluences are of about the same order of magnitude (0.1 to 6 J/cm^2 for ns excitation, and 0.01 to 1 J/cm^2 for fs excitation), the intensity is higher by three to four orders of magnitude with fs excitation (10^7 to 10^9 W/cm^2 for ns excitation, and 10^{11} to 10^{13} W/cm^2 for fs excitation). It is well known that optical fluence as well as optical intensity are determining factors for the nonlinear response of a material. With longer pulsewidths and higher fluences ESA effects will be prominent, while with shorter pulsewidths and higher intensities 2PA effects will be prominent.[49] Therefore in the present case, with ns excitation ESA will be prevalent, and the contribution of 2PA will be relatively small. Hence we can numerically model the transmission of ns pulses using the nonlinear propagation equation [50]

$$\frac{dF}{dz'} = -\alpha F - \left(\frac{\alpha\sigma}{2h\upsilon}\right)F^2 \qquad (1)$$

where F is the input laser fluence and σ is the excited state absorption cross section. z' is the propagation distance within the sample, h is the Planck's constant and ν is the laser

Journal Name

ARTICLE

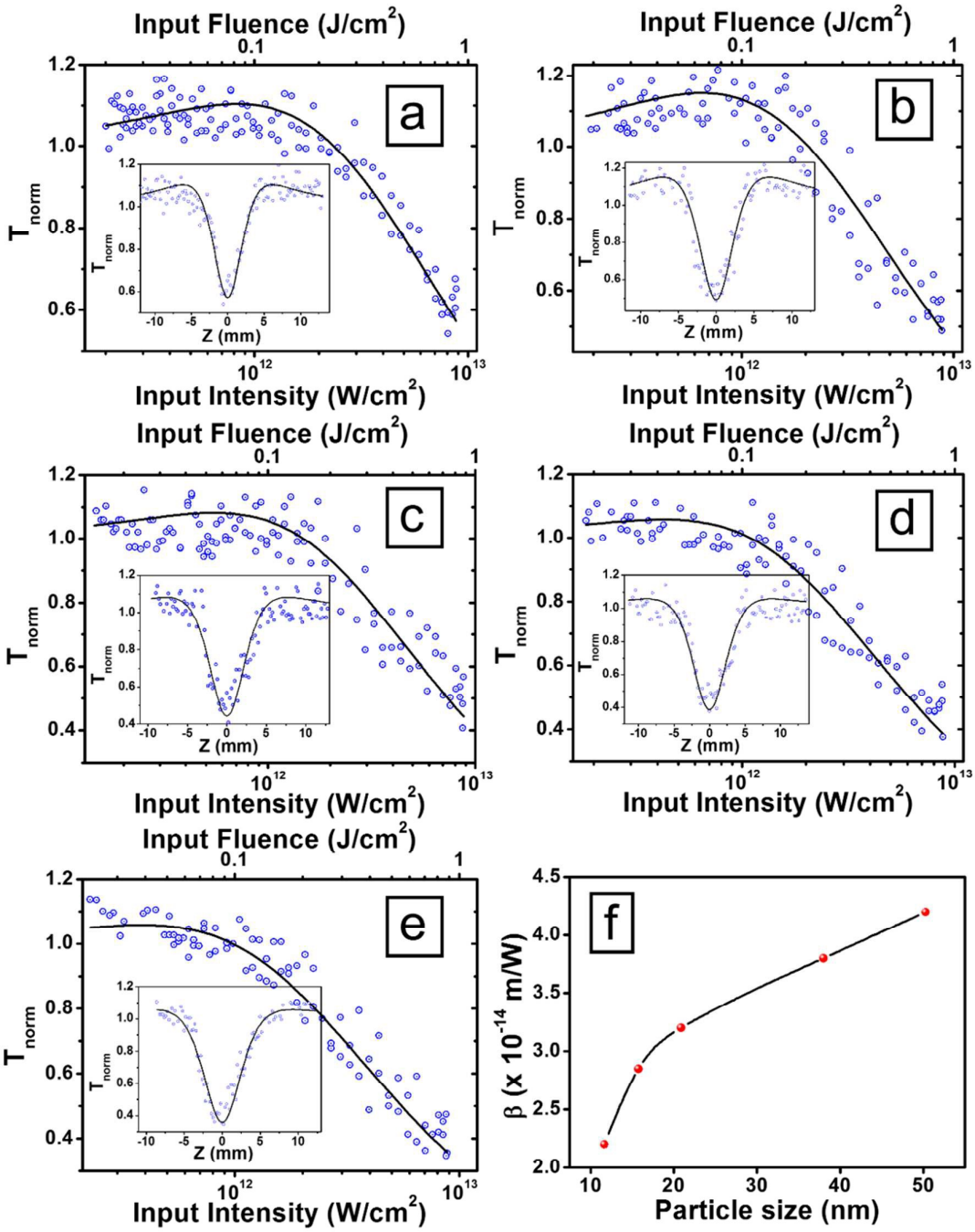

Fig. 5 Normalized transmission of the samples plotted as a function of input fluence and intensity, deduced from the open aperture Z-scans given in the insets. (a) MgF1, (b) MgF2, (c) MgF3, (d) MgF4 and (e) MgF5. Excitation is by 100 fs, 800 nm laser pulses, of energy 7 μJ. Open circles are data points and solid curves are numerical fits to the data using equation 3. (f) Correlation between particle size and two-photon absorption coefficient (β). The line is a guide to the eye.

Journal Name

ARTICLE

frequency (given by c/λ where c is the light velocity and λ is the wavelength). α is the absorption coefficient which is given by $\alpha(F) = \alpha_0/(1 + (F/F_s))$ where F_s is the saturation fluence. Equation 1 can be fitted to the nonlinear transmission data to obtain the values of F_s and σ. Since F_s is given by $h\nu/2\sigma_0$, it is possible to calculate σ_0, the ground state absorption cross section, from the value of F_s which is particularly advantageous in the case of samples whose molar concentrations are not directly known. The nonlinear transmission behaviour will depend on the values of σ/σ_0 and F_s. The value of σ/σ_0 gives the figure of merit for an RSA material.

Table 1. Nonlinear optical parameters calculated by numerically fitting the ns and fs laser pulse transmission data (obtained from the Z-scan curves) to the nonlinear propagation equations 1 and 3, respectively. Particle size is calculated using the Scherrer equation, and band gap energy is determined from the Tauc plots.

Sample Name	Particle Size	Band gap Energy	Excitation Conditions					
			5 ns, 532 nm				100 fs, 800nm	
			σ (cm^2)	F_s (J/cm^2)	σ_0 (cm^2)	σ/σ_0	β (m/W)	I_S (W/m^2)
MgF1	11.66	4.08	1.2×10^{-19}	1.4	1.33×10^{-19}	0.89	2.2×10^{-14}	12.6×10^{13}
MgF2	15.77	3.90	2.2×10^{-19}	7	2.66×10^{-20}	8.24	2.9×10^{-14}	55.3×10^{13}
MgF3	20.88	3.82	3.1×10^{-19}	8.4	2.22×10^{-20}	13.94	3.2×10^{-14}	75.3×10^{13}
MgF4	38.01	3.73	3.3×10^{-19}	10	1.86×10^{-20}	17.66	3.8×10^{-14}	75.3×10^{13}
MgF5	50.27	3.64	3.9×10^{-19}	12	1.55×10^{-20}	25.05	4.2×10^{-14}	12.6×10^{13}

On the other hand the nonlinear absorption of fs pulses is dependent more on the intensity (rather than the fluence), and the nonlinear absorption coefficient can be written in the form

$$\alpha(z) = \frac{\alpha_0}{1+\left(I/I_s\right)} + \beta I \qquad (2)$$

where β is the 2PA coefficient and I_s is the saturation intensity. The corresponding propagation equation is given by

$$\frac{dI}{dz'} = -\left[\alpha_0 \Big/ \left(1+\frac{I}{I_s}\right) + \beta I\right] I \qquad (3)$$

which can be numerically fitted to the fs transmission data to obtain I_s and β values. The calculated nonlinear parameters for both ns and fs excitations are listed in Table 1. From Figs. 4 and 5 it is obvious that the MgF NPs mostly exhibit an absorption saturation behaviour in the low and moderate input regions, which transforms to an ESA (ns) or 2PA (fs) behaviour at higher fluences (intensities). Interestingly, dielectric polarization effects in spinel ferrites that happen due to the exchange of electrons between Fe^{2+} and Fe^{3+},[51] can also contribute to optical nonlinearity.[33] The number of excess Fe^{2+} ions which favour polarization are reported to increase at higher annealing temperatures. We have observed a consistent increase in the σ/σ_0 and β values of MgF NPs sintered at higher temperatures, which could be related to this enhancement in polarization. The optical limiting thresholds calculated for ns excitation are 16 J cm^{-2}, 7.5 J cm^{-2}, 6 J cm^{-2}, 5 J cm^{-2} and 4.2 J cm^{-2} for MgF1, MgF2, MgF3, MgF4 and MgF5, respectively. The optical limiting threshold value of MgF5 NPs in the ns excitation domain is comparable to other magnetic nanomaterials such as Fe_2O_3/g-C_3N_4 NPs,[30] $NiFe_2O_4$,[33] $ZnFe_2O_4$,[34] and Co nanowires.[52] On the other hand the limiting thresholds for fs excitation are lower at 1 J cm^{-2}, 0.82 J cm^{-2}, 0.71 J cm^{-2}, 0.59 J cm^{-2} and 0.53 J cm^{-2} for MgF1, MgF2, MgF3, MgF4 and MgF5, respectively. This shows that in contrast to the limiting of ns pulses, limiting of fs pulses is more of an intensity dependent phenomenon. In addition, the calculated ESA cross sections and 2PA coefficients illustrate a clear dependence of the strength of nonlinear absorption on the particle size: as the size increases the nonlinearity also increases (Fig. 4f and Fig. 5f).

Conclusions

In conclusion, we have investigated the nonlinear optical properties of Magnesium ferrite nanoparticles in the size range of 10-50 nm, synthesized by the sol gel technique. The nanoparticles were characterized using XRD, HRTEM, FESEM, FTIR and UV-Visible spectroscopy. Nonlinear optical measurements were carried out using open aperture Z-scan

technique employing short and ultrashort laser pulses. All samples show moderate absorption saturation at lower input fluences and efficient optical limiting at higher fluences. Optical nonlinearity arises mostly from excited state absorption for nanosecond excitation while two photon absorption is relatively more prominent for femtosecond excitation. The corresponding ESA cross sections and 2PA coefficients have been numerically calculated from measured data. Enhancement in nonlinear absorption is observed for both nanosecond and femtosecond excitations with increase in particle size. These results reveal that the Magnesium ferrite nanoparticles investigated in the present work are useful for designing efficient optical limiter devices for short as well as ultrashort laser pulses. These devices will allow maximum light to be transmitted to an optical detector at low fluences and intensities, while at high fluences and intensities the limiting action will protect the detector from potential damage.

Acknowledgements

KS thanks the DST, Govt. of India for the DST INSPIRE Faculty award. NK acknowledges the funding from DST, Govt. of India through Nanomission to IIUCNN through FIST program and UGC, Govt. of India through SA program to SPAP.

Notes and references

1. T. Bala, C. R. Sankar, M. Baidakova, V. Osipov, T. Enoki, P. A. Joy, B. L. V. Prasad and M. Sastry, *Langmuir*, 2005, **21**, 10638-10643.
2. D. S. Mathew and R.-S. Juang, *Chemical Engineering Journal*, 2007, **129**, 51-65.
3. J. Msomi and T. Moyo, *Journal of Magnetism and Magnetic Materials*, 2009, **321**, 1246-1250.
4. Z. Lixin, L. Jia and C. Qianwang, *Journal of Physics: Condensed Matter*, 2005, **17**, 5095.
5. M. J. Iqbal, Z. Ahmad, Y. Melikhov and I. C. Nlebedim, *Journal of Magnetism and Magnetic Materials*, 2012, **324**, 1088-1094.
6. N. A. Frey, S. Peng, K. Cheng and S. Sun, *Chemical Society Reviews*, 2009, **38**, 2532-2542.
7. Q. Dai, D. Berman, K. Virwani, J. Frommer, P.-O. Jubert, M. Lam, T. Topuria, W. Imaino and A. Nelson, *Nano Letters*, 2010, **10**, 3216-3221.
8. J. Schotter, P. B. Kamp, A. Becker, A. Puhler, D. Brinkmann, W. Schepper, H. Bruckl and G. Reiss, *IEEE Transactions on Magnetics*, 2002, **38**, 3365-3367.
9. C. Xu and S. Sun, *Dalton Transactions*, 2009, DOI: 10.1039/b900272n, 5583-5591.
10. U. Lüders, A. Barthélémy, M. Bibes, K. Bouzehouane, S. Fusil, E. Jacquet, J. P. Contour, J. F. Bobo, J. Fontcuberta and A. Fert, *Advanced Materials*, 2006, **18**, 1733-1736.
11. Y.-w. Jun, J.-H. Lee and J. Cheon, *Angewandte Chemie International Edition*, 2008, **47**, 5122-5135.
12. R. Hao, R. Xing, Z. Xu, Y. Hou, S. Gao and S. Sun, *Advanced Materials*, 2010, **22**, 2729-2742.
13. F. Liu, Y. Hou and S. Gao, *Chemical Society Reviews*, 2014, **43**, 8098-8113.
14. S. Laurent, D. Forge, M. Port, A. Roch, C. Robic, L. Vander Elst and R. N. Muller, *Chemical Reviews*, 2008, **108**, 2064-2110.
15. V. Šepelák, A. Feldhoff, P. Heitjans, F. Krumeich, D. Menzel, F. J. Litterst, I. Bergmann and K. D. Becker, *Chemistry of Materials*, 2006, **18**, 3057-3067.
16. A. Franco and M. S. Silva, *Journal of Applied Physics*, 2011, **109**, 07B505.
17. R. Köferstein, T. Walther, D. Hesse and S. G. Ebbinghaus, *Journal of Materials Science*, 2013, **48**, 6509-6518.
18. M. Goodarz Naseri, M. H. M. Ara, E. B. Saion and A. H. Shaari, *Journal of Magnetism and Magnetic Materials*, 2014, **350**, 141-147.
19. S. Verma, P. A. Joy, Y. B. Khollam, H. S. Potdar and S. B. Deshpande, *Materials Letters*, 2004, **58**, 1092-1095.
20. M. Sheykhan, H. Mohammadnejad, J. Akbari and A. Heydari, *Tetrahedron Letters*, 2012, **53**, 2959-2964.
21. N.-S. Chen, X.-J. Yang, E.-S. Liu and J.-L. Huang, *Sensors and Actuators B: Chemical*, 2000, **66**, 178-180.
22. Y.-L. Liu, Z.-M. Liu, Y. Yang, H.-F. Yang, G.-L. Shen and R.-Q. Yu, *Sensors and Actuators B: Chemical*, 2005, **107**, 600-604.
23. P. P. Hankare, S. D. Jadhav, U. B. Sankpal, R. P. Patil, R. Sasikala and I. S. Mulla, *Journal of Alloys and Compounds*, 2009, **488**, 270-272.
24. S. Reddy, B. E. Kumara Swamy, U. Chandra, K. R. Mahathesha, T. V. Sathisha and H. Jayadevappa, *Analytical Methods*, 2011, **3**, 2792-2796.
25. V. M. Khot, A. B. Salunkhe, N. D. Thorat, M. R. Phadatare and S. H. Pawar, *Journal of Magnetism and Magnetic Materials*, 2013, **332**, 48-51.
26. L. B. Kong, Z. W. Li, G. Q. Lin and Y. B. Gan, *Journal of the American Ceramic Society*, 2007, **90**, 2104-2112.
27. E. S. Kooij, A. C. Gâlcă and B. Poelsema, *Journal of Colloid and Interface Science*, 2006, **304**, 261-270.
28. S. S. Nair, J. Thomas, C. S. Suchand Sandeep, M. R. Anantharaman and R. Philip, *Applied Physics Letters*, 2008, **92**, 171908.
29. T. N. Narayanan, C. S. S. Sandeep, M. M. Shaijumon, P. M. Ajayan, P. Reji and M. R. Anantharaman, *Nanotechnology*, 2009, **20**, 285702.
30. K. Sridharan, T. Kuriakose, R. Philip and T. J. Park, *Applied Surface Science*, 2014, **308**, 139-147.
31. J. P. Huang and K. W. Yu, *Applied Physics Letters*, 2005, **86**, 041905.
32. K. Sridharan, M. Agarwal, J. Philip, T. Endo and R. Philip, *Transactions of the Materials Research Society of Japan*, 2010, **35**, 159-162.
33. J. J. Thomas, S. Krishnan, K. Sridharan, R. Philip and N. Kalarikkal, *Materials Research Bulletin*, 2012, **47**, 1855-1860.
34. P. Chantharasupawong, R. Philip, T. Endo and J. Thomas, *Applied Physics Letters*, 2012, **100**, 221108.
35. V. Šepelák, M. Menzel, K. D. Becker and F. Krumeich, *The Journal of Physical Chemistry B*, 2002, **106**, 6672-6678.
36. C. Suryanarayana and M. G. Norton, in *X-Ray Diffraction: A Practical Approach*, Springer US, Boston, MA, 1998, DOI: 10.1007/978-1-4899-0148-4_9, pp. 207-221.
37. J. Yan, G. Wu, N. Guan, L. Li, Z. Li and X. Cao, *Physical Chemistry Chemical Physics*, 2013, **15**, 10978-10988.
38. K. Sridharan, E. Jang and T. J. Park, *CrystEngComm*, 2013, **15**, 8241-8245.
39. K. Sridharan, N. Roy, R. Philip and T. J. Park, *Journal of Alloys and Compounds*, 2014, **611**, 82-90.
40. J. Tauc, R. Grigorovici and A. Vancu, *physica status solidi (b)*, 1966, **15**, 627-637.
41. G. P. Joshi, N. S. Saxena, R. Mangal, A. Mishra and T. P. Sharma, *Bulletin of Materials Science*, **26**, 387-389.
42. K. B. Modi, M. C. Chhantbar and H. H. Joshi, *Ceramics International*, 2006, **32**, 111-114.
43. A. Pradeep, P. Priyadharsini and G. Chandrasekaran, *Journal of Magnetism and Magnetic Materials*, 2008, **320**, 2774-2779.
44. J. Feng, T. Liu, Y. Xu, J. Zhao and Y. He, *Ceramics International*, 2011, **37**, 1203-1207.

45. S. E. Shirsath, B. G. Toksha, R. H. Kadam, S. M. Patange, D. R. Mane, G. S. Jangam and A. Ghasemi, *Journal of Physics and Chemistry of Solids*, 2010, **71**, 1669-1675.
46. M. Stoia, L. B. Tudoran and P. Barvinschi, *Journal of Thermal Analysis and Calorimetry*, 2013, **113**, 11-19.
47. G. A. Adebayo, Y. Liang, C. R. Miranda and S. Scandolo, *The Journal of Chemical Physics*, 2009, **131**, 014506.
48. I. V. Chernyshova, M. F. Hochella Jr and A. S. Madden, *Physical Chemistry Chemical Physics*, 2007, **9**, 1736-1750.
49. M. Rumi and J. W. Perry, *Adv. Opt. Photon.*, 2010, **2**, 451-518.
50. K. Sridharan, P. Sreekanth, T. J. Park and R. Philip, *The Journal of Physical Chemistry C*, 2015, **119**, 16314-16320.
51. S. S. Bellad, S. C. Watawe and B. K. Chougule, *Materials Research Bulletin*, 1999, **34**, 1099-1106.
52. H. Pan, W. Chen, Y. P. Feng, W. Ji and J. Lin, *Applied Physics Letters*, 2006, **88**, 223106.

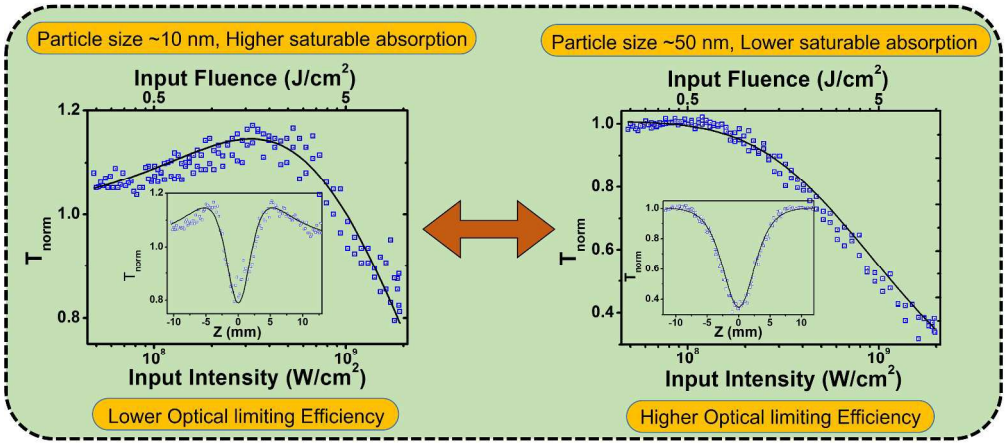

1008x443mm (96 x 96 DPI)